Coherence and mode decomposition of weak twin beams

Jan Peřina Jr.

RCPTM, Joint Laboratory of Optics of Palacký University and Institute of
Physics of Academy of Sciences of the Czech Republic, 17. listopadu 12, 771 46
Olomouc, Czech Republic

E-mail: `jan.perina.jr@upol.cz`

Abstract. Properties of weak spatio-spectral twin beams in paraxial approximation are analyzed using the decomposition into appropriate paired modes. Numbers of paired modes as well as numbers of modes in the signal (or idler) field in the transverse wave-vector and spectral domains are analyzed as functions of pump-beam parameters. Spatial and spectral coherence of weak twin beams is described by auto- and cross-correlation functions. Relation between the numbers of modes and coherence is discussed.

Keywords: twin beam, spatial and spectral coherence, number of modes

1. Introduction

Generation of photon pairs by spontaneous paramet-ric down-conversion [1] belongs to the most frequently studied nonlinear processes in optics. The reason is entanglement of photons constituting a photon pair. It represents a purely quantum property. Entan-glement leads to nonclassical cross-correlation func-tions between the signal and idler fields [2] that in-fluence many physical effects. Nonclassical multiple coincidence-count rates used, e.g., for tests of the Bell inequalities [3, 4] or quantum teleportation [5] repre-sent the most important manifestation of these correla-tions. Unusual entangled two-photon absorption with its entanglement-induced transparency [6, 7] and vir-tual state two-photon spectroscopy [8] is another ex-ample of the large impact of entanglement of photons. Also ghost imaging has to be mentioned here [9]. At present, there already exist several applications based upon entangled photon pairs including quantum key distribution [10], ultra-fast measurements [11] and ab-solute detector calibration [12, 13].

This wide use of entangled photon pairs has naturally stimulated investigations of a detailed structure of photon pairs. It has been shown that their properties are fully described by two-photon (spectral, temporal, spatial) amplitudes at the level of individual photon pairs [14, 15]. Moreover, the Schmidt decomposition of a two-photon amplitude [16, 17] has been found crucial for the quantification of entanglement by the Schmidt number. We note that no physical quantity is directly related to entanglement but entanglement influences even qualitatively the physical behavior of photon pairs. As the experimental determination of the Schmidt number [18, 19] and profiles of the modes [20, 21, 22] is difficult, an alternative approach based on the measurement of field width and width of the corresponding intensity cross-correlation function has been developed giving the Fedorov ratio [23, 24, 25] as a good quantifier of entanglement.

In the last years, a greater deal of attention has been devoted to fields composed of many photon pairs arising in parametric down-conversion [26, 27, 28]. Properties of these twin beams reflect those of the individual photon pairs [29], at least for not very intense twin beams [30]. For characterizing twin beams, auto-correlation functions are important as well as the cross-correlation functions [31]. Auto-correlation functions then give, according to statistical optics [32], the information about the number of modes constituting the signal (or idler) part of the twin beam. In analogy with the definition of Fedorov ratio, this number of modes can be determined by the ratio of field width and width of the corresponding auto-correlation function. Considering weak twin beams, the auto-correlation functions can even be derived from the two-photon amplitudes describing photon pairs.

In this contribution, we determine side by side the spatial and spectral auto- and cross-correlation functions as they depend on pump-field parameters. Using these functions, we obtain the number of modes in the signal (or idler) field and compare it with the Schmidt number giving the number of paired modes [24].

The paper is organized as follows. Theory suitable for describing weak twin beams is presented in Sec. 2. Sec. 3 is devoted to the properties of twin beams in the transverse wave-vector plane. Spectral properties of the twin beams are discussed in Sec. 4. Sec. 5 brings conclusions.

2. Theory of weak twin beams

Parametric down-conversion in a medium with tensor d of the second-order nonlinear coefficients is charac-terized by momentum operator $\hat{G}_{\text{int}}$ written as follows [33, 34]:

$$\hat{G}_{\text{int}}(z) = 4\epsilon_0 \int dx dy \int_{-\infty}^{\infty} dt$$
$$\left[d : E_p^{(+)}(\mathbf{r}, t) \hat{E}_s^{(-)}(\mathbf{r}, t) \hat{E}_i^{(-)}(\mathbf{r}, t) + \text{h.c.} \right]; (1)$$

$\mathbf{r} = (x, y, z)$. Symbol $E_p^{(+)}$ denotes the positive-frequency part of the classical pump electric-field amplitude and $\hat{E}_s^{(-)}$ $[\hat{E}_i^{(-)}]$ means the negative-frequency part of the signal- [idler-] field operator amplitude. Permittivity of vacuum is denoted as ϵ_0, symbol : is shorthand for tensor shortening with respect to its three indices and h.c. replaces the Hermitian conjugated term.

Amplitudes of all three interacting fields can be decomposed into harmonic plane waves with wave vectors $\mathbf{k}_a$ and frequencies ω_a:

$$E_a^{(+)}(\mathbf{r}, t) = \frac{1}{\sqrt{2\pi}^3} \int d\mathbf{k}_a \, E_a^{(+)}(\mathbf{k}_a) \exp(i\mathbf{k}_a\mathbf{r} - i\omega_a t),$$
$$a = p, s, i. \tag{2}$$

In the considered paraxial approximation, the plane wave with wave vector $\mathbf{k}_a$ is conveniently parameterized by its frequency ω_a and transverse wave vector $\mathbf{k}_a^\perp$. The quantum signal and idler spectral electric-field amplitudes $\hat{E}_a^{(-)}(\mathbf{k}_a^\perp, \omega_a)$ can then be expressed in terms of the appropriate creation operators $\hat{a}^\dagger(\mathbf{k}_a^\perp, \omega_a)$:

$$\hat{E}_a^{(-)}(\mathbf{k}_a^\perp, \omega_a) = -i\sqrt{\frac{\hbar\omega_a^2}{2\epsilon_0 c^2 k_a}}\, \hat{a}_a^\dagger(\mathbf{k}_a^\perp, \omega_a); \qquad (3)$$

$\hbar$ is the reduced Planck constant and c is the speed of light in vacuum; $k_a = |\mathbf{k}_a|$.

Correlations in the transverse wave-vector planes of the signal and idler fields are described by the following function T_L depending on the pump-field transverse spatial spectrum $E_p^\perp(\mathbf{k}_p^\perp)$:

$$T_L(\mathbf{k}_s^\perp, \mathbf{k}_i^\perp) = E_p^\perp(\mathbf{k}_s^\perp + \mathbf{k}_i^\perp)$$
$$\times \exp\left(-i\left[\frac{|\mathbf{k}_s^\perp + \mathbf{k}_i^\perp|^2}{2k_p} - \frac{|\mathbf{k}_s^\perp|^2}{2k_s} - \frac{|\mathbf{k}_i^\perp|^2}{2k_i}\right]\frac{L}{2}\right)$$
$$\times \mathrm{sinc}\left(\left[\frac{|\mathbf{k}_s^\perp + \mathbf{k}_i^\perp|^2}{2k_p} - \frac{|\mathbf{k}_s^\perp|^2}{2k_s} - \frac{|\mathbf{k}_i^\perp|^2}{2k_i}\right]\frac{L}{2}\right); \qquad (4)$$

$\mathrm{sinc}(x) \equiv \sin(x)/x$ and δ stands for the Dirac δ-function. In Eq. (4), $|\mathbf{k}_a^\perp|^2 = k_{a,x}^2 + k_{a,y}^2$ and L denotes the crystal length.

We assume that the emitted signal and idler fields have the radial symmetry. This is a good approximation for sufficiently narrow spatial spectral profiles $E_p^\perp$ of the pump field. The pump field in the considered type-I nonlinear interaction propagates as an extraordinary wave and so its index n_p of refraction changes linearly with the radial emission angle ϑ_p [$\vartheta_p = \arcsin(|\mathbf{k}_p^\perp|/k_p)$] in the plane containing the propagation direction and the crystal optical axis. This dependence introduces anisotropy into the generated signal and idler fields [35, 36, 37]. Assuming the Gaussian transverse pulse profile with radius w_p [$E_p^\perp(|\mathbf{k}_p^\perp|) = w_p/\sqrt{2\pi}\exp(-w_p^2|\mathbf{k}_p^\perp|^2/4)$] the anisotropy is well developed for narrow transverse pump profiles with wide spatial spectra. Anisotropy considerably modifies the emitted signal and idler fields for the pump-field radii w_p comparable or smaller than w_p^a (for more details, see [35]):

$$w_p^a = \frac{1}{n_p}\left|\frac{dn_p(\omega_p^0, \vartheta_p)}{d\vartheta_p}\right|\frac{L}{x_e}; \qquad (5)$$

$x_e \approx 2.2$ [$\sin(x_e)/x_e = 1/e$].

The assumed radial symmetry qualitatively simplifies the description as it allows to decompose the function T_L into the dual Schmidt basis in both radial and azimuthal directions in the transverse planes:

$$T_L(\mathbf{k}_s^\perp, \mathbf{k}_i^\perp) = \frac{t^\perp}{2\pi\sqrt{k_s^\perp k_i^\perp}}\sum_{m=-\infty}^\infty\sum_{l=0}^\infty \lambda_{ml}^\perp$$
$$\times t_{s,ml}(k_s^\perp, \varphi_s)t_{i,ml}(k_i^\perp, \varphi_i), \qquad (6)$$

$$t_{s,ml}(k_s^\perp, \varphi_s) = u_{s,ml}(k_s^\perp)\exp(im\varphi_s),$$
$$t_{i,ml}(k_i^\perp, \varphi_i) = u_{i,ml}(k_i^\perp)\exp(-im\varphi_i).$$

Whereas the functions $u_{a,ml}$ describe the radial parts of the fields, the harmonic functions $\exp(im\varphi_a)/\sqrt{2\pi}$ are appropriate for the azimuthal parts of the fields, $a = s, i$. Symbols $\lambda_{ml}^\perp$ denote the Schmidt numbers and $t^\perp$ is the normalization constant.

Unitary transformations of the field operators,

$$\hat{a}_{a,ml}(\omega_a, z) = \int_0^\infty dk_a^\perp \int_0^{2\pi} d\varphi_a\, t_{a,ml}^*(k_a^\perp, \varphi_a)$$
$$\times \hat{a}_a(k_a^\perp, \varphi_a, \omega_a, z), \quad a = s, i, \qquad (7)$$

then allow us to write the first-order perturbation solution of the Schrödinger equation as follows:

$$|\psi\rangle_{\mathrm{out}} = t^\perp\sum_{m,l}\lambda_{ml}^\perp\int_0^\infty d\omega_s\int_0^\infty d\omega_i\, F_L(\omega_s, \omega_i)$$
$$\times \hat{a}_{s,ml}^\dagger(\omega_s, 0)\hat{a}_{i,ml}^\dagger(\omega_i, 0)|\mathrm{vac}\rangle; \qquad (8)$$

$|\mathrm{vac}\rangle$ is the incident vacuum state. The two-photon spectral amplitude F_L introduced in Eq. (8) is determined by the formula

$$F_L(\omega_s, \omega_i) = \frac{2id_{\mathrm{eff}}L}{\sqrt{2\pi}^3 c^2}\frac{\omega_s\omega_i}{\sqrt{k_s k_i}}E_p^\parallel(\omega_s + \omega_i)$$
$$\times \exp\left(-i[k_p(\omega_s + \omega_i) - k_s(\omega_s) - k_i(\omega_i)]L/2\right)$$
$$\times \mathrm{sinc}\left([k_p(\omega_s + \omega_i) - k_s(\omega_s) - k_i(\omega_i)]L/2\right), \qquad (9)$$

where $E_p^\parallel$ stands for the pump-field spectrum and d_{eff} denotes an effective nonlinear coupling constant. The Schmidt decomposition of two-photon amplitude F_L,

$$F_L(\omega_s, \omega_i) = f^\parallel\sum_{q=0}^\infty\lambda_q^\parallel f_{s,q}(\omega_s)f_{i,q}(\omega_i), \qquad (10)$$

and introduction of new field operators $\hat{a}_{a,mlq}$,

$$\hat{a}_{a,mlq} = \int_0^\infty d\omega_a\, f_{a,q}^*(\omega_a)\hat{a}_{a,ml}(\omega_a, 0), \quad a = s, i, \qquad (11)$$

allows to rearrange the output state $|\psi\rangle_{\mathrm{out}}$ into the form:

$$|\psi\rangle_{\mathrm{out}} = t^\perp f^\parallel\sum_{m,l,q}\lambda_{ml}^\perp\lambda_q^\parallel\hat{a}_{s,mlq}^\dagger\hat{a}_{i,mlq}^\dagger|\mathrm{vac}\rangle. \qquad (12)$$

Formula (12) represents the output state $|\psi\rangle_{\mathrm{out}}$ decomposed into independent paired spatial and spectral modes. We note that there occurs degeneracy in the signal and idler mode structure for $m = 0$ owing to the radial and spectral symmetry of the signal and idler fields. Due to this degeneracy, we cannot distinguish a signal and an idler photons in modes with $m = 0$ as both photons are created in one spatio-spectral mode. This considerably modifies properties of the generated paired fields in the collinear geometry [38]. On the other hand, non-collinear geometries are practically unaffected by this degeneracy as the relative

contribution of such photon pairs to the structure of a twin beam is negligible.

The emitted signal (or idler) field is characterized by its intensity profiles along variables $k_a^\perp$, φ_a and ω_a, $a = s, i$. Its internal correlations are described by amplitude correlation functions in these variables. The mutual signal and idler correlations are characterized by intensity cross-correlation functions in these variables. In detail, intensity profile $n_{s,k}$ (expressed in photon-number density) $[n_{s,k}(k_s^\perp) \approx \langle \hat{a}_s^\dagger(k_s^\perp) \hat{a}_s(k_s^\perp) \rangle]$ of the signal field in the radial wave-vector direction is derived from the function T_L given in Eq. (6):

$$n_{s,k}(k_s^\perp) = k_s^\perp \int_0^\infty dk_i^\perp k_i^\perp$$
$$\times |T_L(k_s^\perp, \varphi_s = 0, k_i^\perp, \varphi_i = \pi)|^2. \qquad (13)$$

Using Eq. (9) the signal-field intensity spectrum $n_{s,\omega}$ $[n_{s,\omega}(\omega_s) \approx \langle \hat{a}_s^\dagger(\omega_s) \hat{a}_s(\omega_s) \rangle]$ is given by the formula

$$n_{s,\omega}(\omega_s) = \int_0^\infty d\omega_i |F_L(\omega_s, \omega_i)|^2. \qquad (14)$$

The amplitude signal-field correlations in their radial $[A_{s,k}^a, A_{s,k}^a(k_s^\perp, k_s'^\perp) \approx \langle \hat{a}_s^\dagger(k_s^\perp) \hat{a}_s(k_s'^\perp) \rangle]$, azimuthal $[A_{s,\varphi}^a]$ and spectral $[A_{s,\omega}^a]$ variables are described by the corresponding auto-correlation functions given as:

$$A_{s,k}^a(k_s^\perp, k_s'^\perp) = \sqrt{k_s^\perp k_s'^\perp} \int_0^\infty dk_i^\perp k_i^\perp T_L^*(k_s^\perp, \varphi_s^0 = 0,$$
$$k_i^\perp, \varphi_i^0 = \pi) T_L(k_s'^\perp, \varphi_s^0 = 0, k_i^\perp, \varphi_i^0 = \pi),$$
$$A_{s,\varphi}^a(\varphi_s, \varphi_s') = k_s^{\perp 0} k_i^{\perp 0} \int_0^{2\pi} d\varphi_i T_L^*(k_s^{\perp 0}, \varphi_s, k_i^{\perp 0}, \varphi_i)$$
$$\times T_L(k_s^{\perp 0}, \varphi_s', k_i^{\perp 0}, \varphi_i),$$
$$A_{s,\omega}^a(\omega_s, \omega_s') = \int_0^\infty d\omega_i F_L^*(\omega_s, \omega_i) F_L(\omega_s', \omega_i). \qquad (15)$$

The intensity correlations between the signal and idler fields in their radial $[C_{s,k}, C_{s,k}(k_s^\perp, k_i^\perp) \approx \langle \mathcal{N} : \hat{a}_s^\dagger(k_s^\perp) \hat{a}_s(k_s^\perp) \hat{a}_i^\dagger(k_i^\perp) \hat{a}_i(k_i^\perp) : \rangle$, symbol $\mathcal{N} ::$ mean the normal ordering of field operators], azimuthal $[C_{s,\varphi}]$ and spectral $[C_{s,\omega}]$ variables are characterized by the following cross-correlation functions:

$$C_{s,k}(k_s^\perp, k_i^\perp) = k_s^\perp k_i^\perp |T_L(k_s^\perp, \varphi_s^0 = 0, k_i^\perp, \varphi_i^0 = \pi)|^2,$$
$$C_{s,\varphi}(\varphi_s, \varphi_i) = k_s^{\perp 0} k_i^{\perp 0} |T_L(k_s^{\perp 0}, \varphi_s, k_i^{\perp 0}, \varphi_i)|^2,$$
$$C_{s,\omega}(\omega_s, \omega_i) = |F_L(\omega_s, \omega_i)|^2. \qquad (16)$$

Similar quantities as written in Eqs. (13—16) for the signal field can be defined also for the idler field.

The number of effectively populated paired modes in a twin beam is determined by the Schmidt number K defined as [39, 40]

$$K = \frac{1}{\sum_q \lambda_q^4} \qquad (17)$$

using eigenvalues λ_q of the Schmidt decomposition of two-photon amplitude normalized such that $\sum_q \lambda_q^2 = 1$.

On the other hand, the number K_b^Δ of modes constituting field b, $b = s, i$, in a given variable is quantified by the ratio of appropriate intensity width Δn_b of field b and width ΔA_b^a of the amplitude auto-correlation function introduced in Eq. (15):

$$K_b^\Delta = \frac{\Delta n_b}{\Delta A_b^a}, \qquad b = s, i. \qquad (18)$$

3. Spatial properties of weak twin beams

We consider a BBO crystal 8-mm long cut for non-collinear type-I process (eoo) for the spectrally-degenerate interaction among the wavelengths $\lambda_p^0 = 349$ nm and $\lambda_s^0 = \lambda_i^0 = 698$ nm ($\vartheta_{\mathrm{BBO}} = 36.3$ deg). The pump field is provided by the third harmonics of the Nd:YLF laser at the wavelength 1.047 μm. Both the Gaussian transverse profile with radius w_p and the Gaussian spectrum of the pump pulse with duration τ_p $[E_p^\parallel(\omega_p) = \sqrt{\tau_p/\sqrt{2\pi}} \exp(-\tau_p^2(\omega_p - \omega_p^0)^2/4)]$ are considered in the calculations. Assuming the pump field at normal incidence, the signal and idler fields at the central frequencies ω_s^0 and ω_i^0 propagate outside the crystal under the radial emission angles $\vartheta_s = \vartheta_i = 8.45$ deg. As this configuration is symmetric with respect to the exchange of the signal and idler fields, we restrict our discussion to only the signal field. We assume in the discussion that the conditions are such that the spectral and spatial properties of the twin beams factorize.

We first pay attention to the properties of twin beams in the wave-vector transverse plane. We assume in accord with the developed model that the twin beam has the rotational symmetry around the z axis and so it is stationary in the azimuthal angle φ. Formula (5) suggests that the rotational symmetry is roughly observed for the pump-field radius w_p larger than w_p^a that equals 270 μm for the 8-mm long crystal and the considered geometry $[n_p = 1.658, |dn_p/d\vartheta_p| = 0.123]$. The pump-field radius w_p is the crucial parameter that determines the properties of twin beams in the transverse plane. It gives the number $K_{k\varphi}$ of independent transverse modes comprising the twin beam. In our configuration, the greater the value of radius w_p the greater the number $K_{k\varphi}$ of independent modes, as documented in Fig. 1. The number $K_{k\varphi}$ of overall modes in the transverse wave-vector plane can approximately be factorized into the number K_k of modes in the radial direction and the number K_φ of modes in the azimuthal direction. This factorization arises from the fact that the number K of radial modes determined for a fixed value of the azimuthal number m depends only weakly on the number m. The
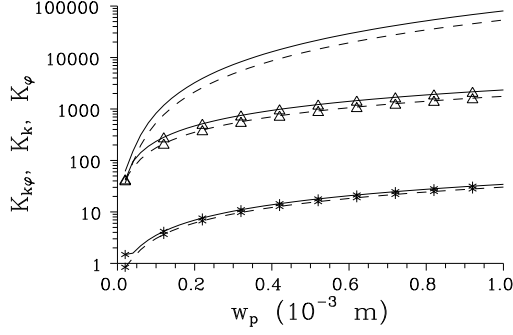
Figure 1. Number $K_{k\varphi}$ of modes in the transverse wave-vector plane (plain curve), number K_k of modes in radial direction (solid curve with $*$) and number K_φ of modes in azimuthal direction (solid curve with $\triangle$) as functions of pump-field radius w_p. Dashed curves give the corresponding numbers K_s^Δ of signal-field modes determined by Eq. (18).
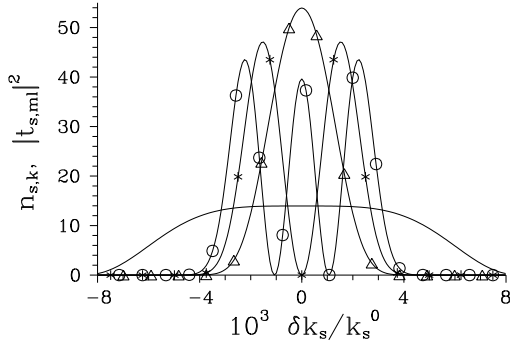
Figure 2. Radial intensity profile $n_{s,k}$ (plain curve) and intensity profiles $|t_{s,0l}|^2$ of modes for $l = 0$ (solid curve with $\triangle$), $l = 1$ (solid curve with $*$) and $l = 2$ (solid curve with $\circ$) in radial direction of the signal field; $w_p = 1 \times 10^{-3}$ m. Functions are normalized such that $\int dk_s n_{s,k}(k_s)/k_s^0 = 1$ and $\int dk_s |t_{s,0l}(k_s)|^2/k_s^0 = 1$.

number K_φ of azimuthal modes is much larger than the number K_k of radial modes as these modes cover the whole circle. There typically occur hundreds or thousands of independent azimuthal modes. On the other hand, from several up to several tens of radial modes are needed for the description of a typical twin beam. Whereas the azimuthal modes take the form of harmonic functions, damped exponential functions modified by oscillating polynomials [41] approximate the radial modes. The first couple of radial modes for $m = 0$ are shown in Fig. 2 together with the radial intensity profile $n_{s,k}$ for the pump field 1-mm wide. It holds that the intensity profile of an l-th radial mode has l zeroes and $l + 1$ local peaks. Also the larger the value of l, the wider the mode. However and importantly, all modes are distributed along the whole intensity profile $n_{s,k}(k_s)$. We note that, in Fig. 1, for the values of pump-field radius w_p smaller than 0.270 μm the generated twin beams are influenced by the crystal anisotropy. Anisotropy leads in general to
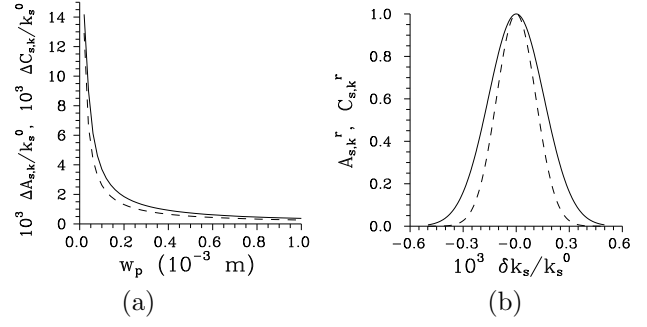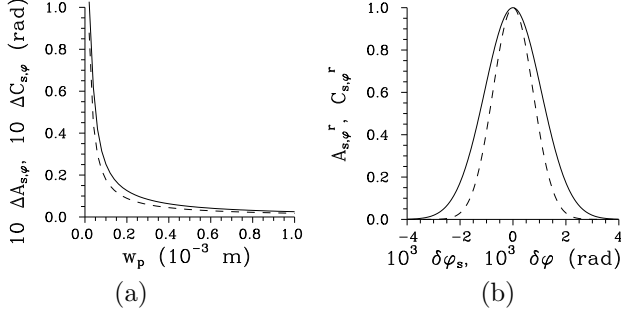

Figure 3. (a) Widths $\Delta A_{s,k}$ (FWHM, full width at half maximum) of signal-field intensity auto-correlation function (plain curve) and $\Delta C_{s,k}$ of intensity cross-correlation function (dashed curve) in radial direction as they depend on pump-field radius w_p. In (b), functions $A_{s,k}^r(\delta k_s) \equiv A_{s,k}(k_s^0 + \delta k_s, k_s^0)/A_{s,k}(k_s^0, k_s^0)$ and $C_{s,k}^r(\delta k_s) \equiv C_{s,k}(k_s^0 + \delta k_s, k_i^0)/C_{s,k}(k_s^0, k_i^0)$ are plotted for $w_p = 1 \times 10^{-3}$ m.

more strict phase-matching conditions which results in greater values of the Schmidt numbers K compared to those shown in Fig. 1. Anisotropy and its role in photon-pair generation has been discussed in detail in [35].

Numbers K_s^Δ of modes in the signal field determined along Eq. (18) are compared with the numbers K of paired modes from the Schmidt decomposition in Fig. 1. This comparison reveals that the values of K^Δ are only approx. by 40% lower than the values of K. The numbers K^Δ of effectively populated signal-field modes are in general smaller than the corresponding Schmidt numbers K as the widths of auto-correlation functions occurring in definition (18) are not able to fully take into account the complex structure of entanglement present in a twin beam [18, 19]. In other words, numbers K of paired modes and numbers K_s^Δ of signal-field modes are defined differently. However, their comparison done in Fig. 1 clearly reveals that both of them are suitable for quantifying the dimensionality of a twin beam.

As the range of radial angles ϑ_s belonging to the emitted photons practically does not change with the pump-field radius w_p and the allowed azimuthal emission angles φ_s lie in interval $(0, 2\pi)$, an increase of the number $K_{s,k\varphi}^\Delta$ of signal-field modes with the radius w_p is caused by the decrease of the radial and azimuthal widths of effective modes given by the extension of amplitude auto-correlation functions $A_{s,k}^a$ and $A_{s,\varphi}^a$ defined in Eqs. (15). The dependence of widths $\Delta A_{s,k}$ and $\Delta A_{s,\varphi}$ of their intensity counterparts on the radius w_p is shown in Figs. 3(a) and 4(a), respectively, and confirms this behavior. Profiles $A_{s,k}$ and $A_{s,\varphi}$ giving the signal-field intensity correlations for the pump field 1-mm wide are drawn in Figs. 3(b) and 4(b).

The generation of signal and idler fields by photon pairs strongly correlated in the transverse plane results

Figure 4. (a) Widths $\Delta A_{s,\varphi}$ (FWHM) of signal-field intensity auto-correlation function (plain curve) and $\Delta C_{s,\varphi}$ of intensity cross-correlation function (dashed curve) in azimuthal direction depending on pump-field radius w_p. In (b), intensity auto-correlation function $A_{s,\varphi}^r(\delta\varphi_s) \equiv A_{s,\varphi}(\varphi_s^0 + \delta\varphi_s, \varphi_s^0)/A_{s,\varphi}(\varphi_s^0, \varphi_s^0)$ valid for an arbitrary angle φ_s^0 and cross-correlation function $C_{s,\varphi}^r(\delta\varphi) \equiv C_{s,\varphi}(\varphi_s^0 + \delta\varphi, \varphi_i^0)/C_{s,\varphi}(\varphi_s^0, \varphi_i^0)$ given for arbitrary angles fulfilling $\varphi_i^0 = \varphi_s^0 + \pi$ are shown for $w_p = 1 \times 10^{-3}$ m.

in strong cross-correlations between the intensities of the signal and idler fields. Also these cross-correlations described by the cross-correlation functions $C_{s,k}$ and $C_{s,\varphi}$ given in Eqs. (16) depend strongly on the pump-field radius w_p. The larger the radius w_p the smaller the widths $\Delta C_{s,k}$ and $\Delta C_{s,\varphi}$ of intensity cross-correlation functions in the radial and azimuthal directions, respectively [see Figs. 3(a) and 4(a)] [42, 31]. The comparison of widths $\Delta C_{s,k}$ and $\Delta A_{s,k}$ (or $\Delta C_{s,\varphi}$ and $\Delta A_{s,\varphi}$) plotted in Figs. 3(a) and 4(a) reveals that the intensity cross-correlation functions are narrower than the intensity auto-correlation functions. This behavior can qualitatively be explained as follows. Cross-correlations are formed by individual photon pairs with certain correlations between the signal and idler photons. As these correlations reflect the geometry of the nonlinear process, blurring of the ideal point-like correlations (in the transverse wave-vector space) occurs. On the other hand, intensity auto-correlations in the signal (or idler) field are created at the quantum level by at least two photon pairs. Roughly speaking, the first emitted photon pair provides a signal photon and its correlated idler twin. The annihilation of the second photon pair using the already present idler photon then creates photon-photon auto-correlations in the signal field. As we need two photon pairs in this reasoning, the overall blurring is larger compared to that of one photon pair. As a consequence, the intensity auto-correlation functions are wider than the intensity cross-correlation functions. Also similarity of the profiles of intensity auto-correlation functions $A_{s,k}$ and $A_{s,\varphi}$ and intensity cross-correlation functions $C_{s,k}$ and $C_{s,\varphi}$, respectively, can be deduced from this reasoning. The curves plotted in Figs. 3(b) and 4(b) confirm this behavior.
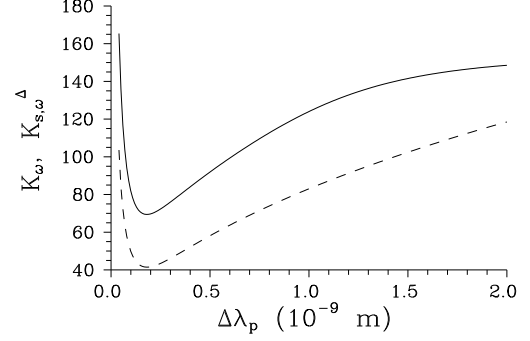

Figure 5. Number K_ω of spectral modes depending on pump-field spectral width $\Delta\lambda_p$; $\Delta\lambda_p = 4\pi\sqrt{2\ln(2)}c/[(\omega_p^0)^2\tau_p]$. Dashed curve gives the number $K_{s,\omega}^\Delta$ of modes according to Eq. (18).

4. Spectral properties of weak twin beams

The behavior of twin beam in the spectral domain and under the considered conditions is more complex compared to the spatial domain. The number K_ω of paired spectral modes attains its minimum when considered as a function of the pump-field spectral width $\Delta\lambda_p$ [24]. The number K_ω of paired spectral modes is larger ($K_\omega \approx 70$) even in this minimum reached for the pump pulse with the spectrum approx. 0.2 nm wide, as documented in Fig. 5. It holds also in the spectral domain that the number K_ω^Δ of signal-field modes determined from the ratio defined in Eq. (18) is smaller than the number K_ω of paired modes arising from the Schmidt decomposition (see Fig. 5). The comparison of curves in Fig. 5 confirms that both the number K_ω of paired modes and the number K_ω^Δ of signal-field modes are suitable for quantifying dimensionality of the twin beam in a broad range of pump-field spectral widths.

The dependence of the number K_ω^Δ of signal-field modes on the pump-field spectral width $\Delta\lambda_p$ as drawn in Fig. 5 can be explained by the behavior of spectral intensity width $\Delta n_{s,\omega}$ and width $\Delta A_{s,\omega}$ of intensity auto-correlation function. Whereas the spectral intensity width $\Delta n_{s,\omega}$ monotonically increases as a function of $\Delta\lambda_p$ [see Fig. 6(a)], the width $\Delta A_{s,\omega}$ of intensity auto-correlation function increases for lower values of $\Delta\lambda_p$ and then it saturates [see Fig. 6(b)]. This results in an increase of the values of K_ω^Δ for larger values of $\Delta\lambda_p$ observed in Fig. 5. Modes of the spectral decomposition behave in the same manner as the modes in the radial direction. Thus, the intensity profile of a q-th mode has q zeros and $q + 1$ peaks and extends over all frequencies found in the spectrum [see Fig. 7(a)]. As a consequence of the conservation law of energy, the frequencies of the emitted signal and idler photons are correlated within the spectral interval given by the pump-field spectral width. However,
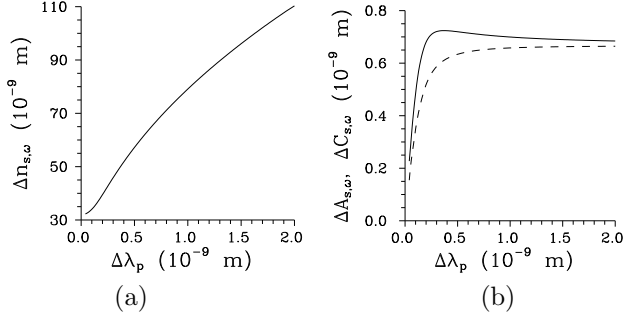
Figure 6. (a) Width $\Delta n_{s,\omega}$ (FWHM) of signal-field intensity spectrum and (b) widths $\Delta A_{s,\omega}$ (FWHM) of signal-field intensity auto-correlation function (plain curve) and $\Delta C_{s,\omega}$ of intensity cross-correlation function (dashed curve) as they depend on pump-field spectral width $\Delta\lambda_p$.
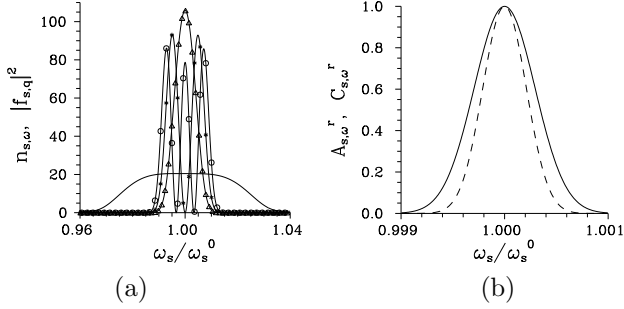
Figure 7. (a) Spectral intensity $n_{s,\omega}$ (plain curve) and spectral intensities $|f_{s,q}|^2$ of modes for $q = 0$ (solid curve with $*$), $q = 1$ (solid curve with $\triangle$) and $q = 2$ (solid curve with $\circ$) in the signal field. (b) Signal-field spectral intensity auto-correlation function $A_{s,\omega}^r(\omega_s) \equiv A_{s,\omega}(\omega_s, \omega_s^0)/A_{s,\omega}(\omega_s^0, \omega_s^0)$ (plain curve) and cross-correlation function $C_{s,\omega}^r(\omega_s) \equiv C_{s,\omega}(\omega_s, \omega_i^0)/C_{s,\omega}(\omega_s^0, \omega_i^0)$ (dashed curve); $\Delta\lambda_p = 1 \times 10^{-10}$ m. Normalization is such that $\int d\omega_s n_{s,\omega}(\omega_s)/\omega_s^0 = 1$ and $\int d\omega_s |f_{s,q}(\omega_s)|^2/\omega_s^0 = 1$.

the interval of correlations is also influenced by the phase-matching conditions that limit its extension. It follows that a certain width of this interval is reached with the increasing pump-field spectral width $\Delta\lambda_p$ and no further increase is possible [see Fig. 6(b)]. This determines correlations between the intensities of the signal and idler fields as well as among the intensities inside the individual fields. The same argumentation as that used in the transverse wave-vector domain shows that the intensity auto-correlation function $A_{s,\omega}$ has to be broader than the intensity cross-correlation function $C_{s,\omega}$ [compare the curves in Fig. 6(b)] and also that profiles of these correlation functions plotted in Fig. 7(b) are similar.

The picture that the overall spectrum is composed of adjacent independent 'local' modes is useful in predicting the behavior of numbers K_ω of paired modes and $K_{s,\omega}^\Delta$ of signal-field modes with respect to spectral filtering. It suggests that the narrower the filter width is, the lower the numbers K_ω and $K_{s,\omega}^\Delta$ of modes needed in the description of a twin beam. This behavior

has been confirmed numerically. A sufficiently strong filtering then allows to reach a twin beam with the number of modes approaching one [43]. The same conclusions are valid for the geometric filtering that reduces the numbers $K_{k\varphi}$ and $K_{s,k\varphi}^\Delta$ of modes in the transverse wave-vector plane.

5. Conclusions

Weak spatio-spectral twin beams have been analyzed in paraxial approximation using the perturbation solution of the Schrödinger equation and its decomposition into the spatial and spectral paired modes. Applying these modes, coherence properties of weak twin beams have been studied using both the auto- and cross-correlation functions. Numbers of paired modes revealed by the Schmidt decomposition and numbers of modes constituting the signal (or idler) field and given by the ratio of field width and width of the appropriate amplitude auto-correlation function have been found mutually proportional in the broad area of the analyzed pump-field parameters. This justifies both of them as appropriate quantifiers of dimensionality of weak twin beams. Whereas the number of transverse modes increases with the increasing pump-field radius in our configuration, the number of spectral modes considered as a function of pump-field spectral width has a well-formed minimum. This behavior has been explained analyzing the widths of appropriate correlation functions. It has been shown that the spectral and transverse wave-vector cross-correlation functions are broader than the corresponding auto-correlation functions.

References

[1] R. W. Boyd. *Nonlinear Optics, 2nd edition.* Academic Press, New York, 2003.
[2] L. Mandel and E. Wolf. *Optical Coherence and Quantum Optics.* Cambridge Univ. Press, Cambridge, 1995.
[3] G. Weihs, T. Jennewein, C. Simon, H. Weinfurter, and A. Zeilinger. Violation of Bell's inequality under strict Einstein locality conditions. *Phys. Rev. Lett.*, 81:5039—5043, 1998.
[4] M. Genovese. Research on hidden variable theories: A review of recent progresses. *Phys. Rep.*, 413:319—396, 2005.
[5] D. Bouwmeester, J. W. Pan, K. Mattle, M. Eibl, H. Weinfurter, and A. Zeilinger. Experimental quantum teleportation. *Nature*, 390:575–579, 1997.

[6] H.-B. Fei, B. M. Jost, S. Popescu, B. E. A. Saleh, and M. C. Teich. Entanglement-induced two-photon transparency. *Phys. Rev. Lett.*, 78:1679—1682, 1997.

[7] J. Peřina Jr., B. E. A. Saleh, and M. C. Teich. Multiphoton absorption cross section and virtual-state spectroscopy for the entangled n-photon state. *Phys. Rev. A*, 57:3972—3986, 1998.

[8] B. E. A. Saleh, B. M. Jost, H.-B. Fei, and M. C. Teich. Entangled-photon virtual-state spectroscopy. *Phys. Rev. Lett.*, 80:3483–3486, 1998.

[9] A. Gatti, E. Brambilla, and L. Lugiato. Quantum imaging. In E. Wolf, editor, *Progress in Optics, Vol. 51*, pages 251—348. Elsevier, Amsterdam, 2008.

[10] N. Gisin, G. Ribordy, W. Tittel, and H. Zbinden. Quantum cryptography. *Rev. Mod. Phys.*, 74:145—195, 2011.

[11] S. Carrasco, J. P. Torres, L. Torner, A. V. Sergienko, B. E. A. Saleh, and M. C. Teich. Enhancing the axial resolution of quantum optical coherence tomography by chirped quasi-phase matching. *Opt. Lett.*, 29:2429–2431, 2004.

[12] D. N. Klyshko. Use of two-photon light for absolute calibration of photoelectric detectors. *Kvantovaya Elektron. (Moscow)*, 7:1932—1940, 1980.

[13] J. Peřina Jr., O. Haderka, M. Hamar, and V. Michálek. Absolute detector calibration using twin beams. *Opt. Lett.*, 37:2475—2477, 2012.

[14] M. H. Rubin, D. N. Klyshko, Y. H. Shih, and A. V. Sergienko. Theory of two-photon entanglement in type-II optical parametric down-conversion. *Phys. Rev. A*, 50:5122—5133, Dec 1994.

[15] J. Peřina Jr., A. V. Sergienko, B. M. Jost, B. E. A. Saleh, and M. C. Teich. Dispersion in femtosecond entangled two-photon interference. *Phys. Rev. A*, 59:2359—2368, 1999.

[16] C. K. Law, I. A. Walmsley, and J. H. Eberly. Continuous frequency entanglement: Effective finite Hilbert space and entropy control. *Phys. Rev. Lett.*, 84:5304—5307, 2000.

[17] C. K. Law and J. H. Eberly. Analysis and interpretation of high transverse entanglement in optical parametric down-conversion. *Phys. Rev. Lett.*, 92:127903, 2004.

[18] K. W. Chan, J. P. Torres, and J. H. Eberly. Transverse entanglement migration in Hilbert space. *Phys. Rev. A*, 75:050101(R), 2007.

[19] F. Just, A. Cavanna, M. V. Chekhova, and G. Leuchs. Transverse entanglement of biphotons. *New J. Phys.*, 15:083015, 2013.

[20] A. Christ, K. Laiho, A. Eckstein, K. N. Cassemiro, and C. Silberhorn. Probing multimode squeezing with correlation functions. *New J. Phys.*, 13:033027, 2011.

[21] I. B. Bobrov, S. S. Straupe, E. V. Kovlakov, and S. P. Kulik. Schmidt-like coherent mode decomposition and spatial intensity correlations of thermal light. *N. J. Phys.*, 15:073016, 2013.

[22] A. Avella, G. Brida, I. P. Degiovanni, M. Genovese, M. Gramegna, L. Lolli, E. Monticone, C. Portesi, M. Rajteri, M. L. Rastello, E. Taralli, P. Traina, and M. White. Self consistent, absolute calibration technique for photon number resolving detectors. *Opt. Express*, 19:23249—23257, 2011.

[23] M. V. Fedorov, M. A. Efremov, A. E. Kazakov, K. W. Chan, C. K. Law, and J. H. Eberly. Spontaneous emission of a photon: Wave-packet structures and atom-photon entanglement. *Phys. Rev. A*, 72:032110, 2005.

[24] Y. M. Mikhailova, P. A. Volkov, and M. V. Fedorov. Biphoton wave packets in parametric down-conversion: Spectral and temporal structure and degree of entanglement. *Phys. Rev. A*, 78:062327, 2008.

[25] G. Brida, V. Caricato, M. V. Fedorov, M. Genovese, M. Gramegna, and S. P. Kulik. Characterization of spectral entanglement of spontaneous parametric-down conversion biphotons in femtosecond pulsed regime. *Eur. Phys. Lett.*, 87:64003, 2009.

[26] O. Haderka, J. Peřina Jr., M. Hamar, and J. Peřina. Direct measurement and reconstruction of nonclassical features of twin beams generated in spontaneous parametric down-conversion. *Phys. Rev. A*, 71:033815, 2005.

[27] M. Bondani, A. Allevi, G. Zambra, M. G. A. Paris, and A. Andreoni. Sub-shot-noise photon-number correlation in a mesoscopic twin beam of light. *Phys. Rev. A*, 76:013833, 2007.

[28] O. Jedrkiewicz, A. Gatti, E. Brambilla, and P. Di Trapani. Experimental observation of a skewed X-type spatiotemporal correlation of ultrabroadband twin beams. *Phys. Rev. Lett.*, 109:243901, 2012.

[29] L. Caspani, E. Brambilla, and A. Gatti. Tailoring the spatiotemporal structure of biphoton entanglement in type-I parametric down-conversion. *Phys. Rev. A*, 81:033808, 2010.

[30] A. Allevi, O. Jedrkiewicz, E. Brambilla, A. Gatti, J. Perina Jr., O. Haderka, and M. Bondani. Coherence properties of high-gain twin beams. *Phys. Rev. A*, 90:06381, 2014.

[31] R. Machulka, O. Haderka, J. Peřina Jr, M. Lamperti, A. Allevi, and M. Bondani. Spatial properties of twin-beam correlations at low- to high-intensity transition. *Opt. Express*, 22:13374—13379, 2014.

[32] J. Peřina. *Coherence of Light*. Kluwer, Dordrecht, 1985.

[33] J. Peřina. *Quantum Statistics of Linear and Nonlinear Optical Phenomena*. Kluwer, Dordrecht, 1991.

[34] J. Peřina Jr. and J. Peřina. Quantum statistics of nonlinear optical couplers. In E. Wolf, editor, *Progress in Optics, Vol. 41*, pages 361—419. Elsevier, Amsterdam, 2000.

[35] M. V. Fedorov, M. A. Efremov, P. A. Volkov, E. V. Moreva, S. S. Straupe, and S. P. Kulik. Spontaneous parametric down-conversion: Anisotropical and anomalously strong narrowing of biphoton momentum correlation distributions. *Phys. Rev. A*, 77:032336, 2008.

[36] M. V. Fedorov, M. A. Efremov, P. A. Volkov, E. V. Moreva, S. S. Straupe, and S. P. Kulik. Anisotropical and high entanglement of biphoton states generated in spontaneous parametric down-conversion. *Phys. Rev. Lett.*, 99:053601, 2007.

[37] C. I. Osorio, G. Molina-Terriza, B. G. Font, and J. P. Torres. Azimuthal distinguishability of entangled photons generated in spontaneous parametric down-conversion. *Opt. Express*, 15:14636—14643, 2007.

[38] M. V. Fedorov and M. I. Miklin. Schmidt modes and entanglement. *Contemporary Phys.*, 55:94—109, 2014.

[39] A. B. U'Ren, K. Banaszek, and I. A. Walmsley. Photon engineering for quantum information processing. *Quantum Inf. Comp.*, 3:480—502, 2003.

[40] A. Gatti, T. Corti, E Brambilla, and D. B. Horoshko. Dimensionality of the spatiotemporal entanglement of parametric down-conversion photon pairs. *Phys. Rev. A*, 86:053803, 2012.

[41] J. Peřina Jr. Quantum properties of counterpropagating two-photon states generated in a planar waveguide. *Phys. Rev. A*, 77:013803, 2008.

[42] M. Hamar, J. Peřina Jr., O. Haderka, and V. Michálek. Transverse coherence of photon pairs generated in spontaneous parametric down-conversion. *Phys. Rev. A*, 81:043827, 2010.

[43] A. M. Pérez, T. S. Iskhakov, P. Sharapova, S. Lemieux, O. V. Tikhonova, M. V. Chekhova, and G. Leuchs. Bright squeezed-vacuum source with 1.1 spatial mode. *Opt. Lett.*, 39:2403—2406, 2014.